Available online at www.sciencedirect.com
SCIENCE DIRECT®
Journal of Sound and Vibration 293 (2006) 360–379
JOURNAL OF SOUND AND VIBRATION
www.elsevier.com/locate/jsvi

Parametric instability of a circular ring subjected to moving springs

Sripathi Vangipuram Canchi, Robert G. Parker*

Department of Mechanical Engineering, Ohio State University, 650 Ackerman Road, Columbus, OH-43202, USA

Received 29 December 2004; received in revised form 7 September 2005; accepted 4 October 2005
Available online 27 December 2005

Abstract

This work investigates parametric instabilities of in-plane bending vibrations of a thin elastic ring subject to forces from discrete rotating springs of arbitrary number, spacing, and orientation. Several configurations are examined, including systems with symmetric and asymmetric circumferential spring spacing, and systems with and without fixed springs. The method of multiple scales is applied to analytically identify principal and combination instability boundaries as closed-form expressions. Two different numerical approaches are used to verify the analytical results. The effects of different system parameters on the instability boundaries are studied analytically: the bending stiffness of the ring, the number of springs, and their stiffness, location, orientation and rotation speed. For several cases, well-defined properties for the occurrence or suppression of instabilities are obtained as simple relations in the system parameters.

1. Introduction

The present work addresses parametric excitation of bending vibrations in a stationary, thin ring subjected to forces from rotating springs. The motivation is from planetary gears, which are commonly used in automotive transmissions, helicopters, aircrafts and wind turbines. Planetary gear dynamics have historically been analyzed using lumped-parameter models that take the ring, planets, carrier and the sun as rigid bodies and the gear tooth meshes as springs. Recent studies, however, indicate that the deformable nature of the gear bodies, especially the ring gear, must be incorporated to accurately model the mechanics. In planetary gears, it is desirable to make the ring gear thin, due to power density and load sharing considerations. This makes the ring flexible, and it deflects significantly due to mesh forces from the rotating planets. These meshes are commonly modeled as elastic springs representing the gear tooth compliance. Bending vibrations of the ring are parametrically excited by forces from the moving springs (ring-planet meshes), causing instability under certain conditions. Similar vibration problems can occur in high-speed bearings where the outer and inner races (rings) are parametrically excited by moving forces from rolling elements.

The vibration of rings has been an area of interest for a long time. The bending vibrations of a circular ring were studied by Hoppe [1], and Love [2] presented frequency expressions for the in-plane bending,

*Corresponding author. Tel.: +1 614 688 3922; fax: +1 614 292 3163.
E-mail address: parker.242@osu.edu (R.G. Parker).

0022-460X/$ - see front matter © 2005 Elsevier Ltd. All rights reserved.
doi:10.1016/j.jsv.2005.10.007

out-of-plane bending, torsional and extensional vibrations of a circular ring. Considerable literature on the free vibrations of thin and thick rings is available accounting for the effects of nonlinearities, shear deformation, and rotatory inertia on in-plane and out-of-plane vibrations [3–6]. Simple frequency expressions accounting for shear and rotatory inertia effects were developed by Kirkhope [7,8], and these were validated against experiments of Kuhl [9] and Lincoln and Volterra [10]. For rings on uniformly distributed elastic foundations, three-dimensional vibrations were studied by Rao [11]. Recently, Wu and Parker studied the vibration of rings on arbitrarily spaced, discrete spring supports [12].

Little work on the vibration of rings subject to moving loads is found in the literature. Huang and Soedel [13,14] presented closed-form solutions for the forced vibration of rotating rings subjected to harmonic and periodic point forces and spatially distributed forces. They compared those results with the inverted problem of a stationary ring with a moving point force. Metrikine and Tochilin [15] studied the vibrations of an elastic ring with a time-varying, moving point force to model train wheels. While beam and disk vibrations with moving springs have been studied extensively [16–21], there seems to be no prior work on the vibration of rings subjected to forces from moving springs. A ring subjected to moving springs manifests as a parametrically excited system because the stiffness operator of the governing equation changes as the spring locations change. In this work, assuming that the moving spring stiffnesses are small compared to the bending stiffness of the ring, perturbation methods are employed to analytically identify parametric instability boundaries as closed-form expressions. For certain cases with symmetry, several instabilities are suppressed. The occurrence or suppression of instabilities is governed by simple relations in the system parameters. Numerical results validating the analytical results are presented.

2. Problem formulation

Fig. 1(a) shows a stationary, thin ring of uniform cross-section with mean radius r subject to forces at its centroidal surface from M multiple spring-sets, $j = 1, 2, \ldots, M$. Each spring-set consists of two springs of constant stiffness k_{1j} and k_{2j} oriented in mutually perpendicular directions. The orientation angle β_j $(0 \leqslant \beta_j < \pi/2)$ is the angle between the spring k_{2j} and the radial direction. The spring-sets are arbitrarily spaced so that ϕ_j $(0 \leqslant \phi_j < 2\pi)$ is the angular coordinate of the jth spring-set measured from fixed $\mathbf{E_1}$ at initial time $t = 0$. All angles are measured positive in the counter-clockwise direction. The above system describes the

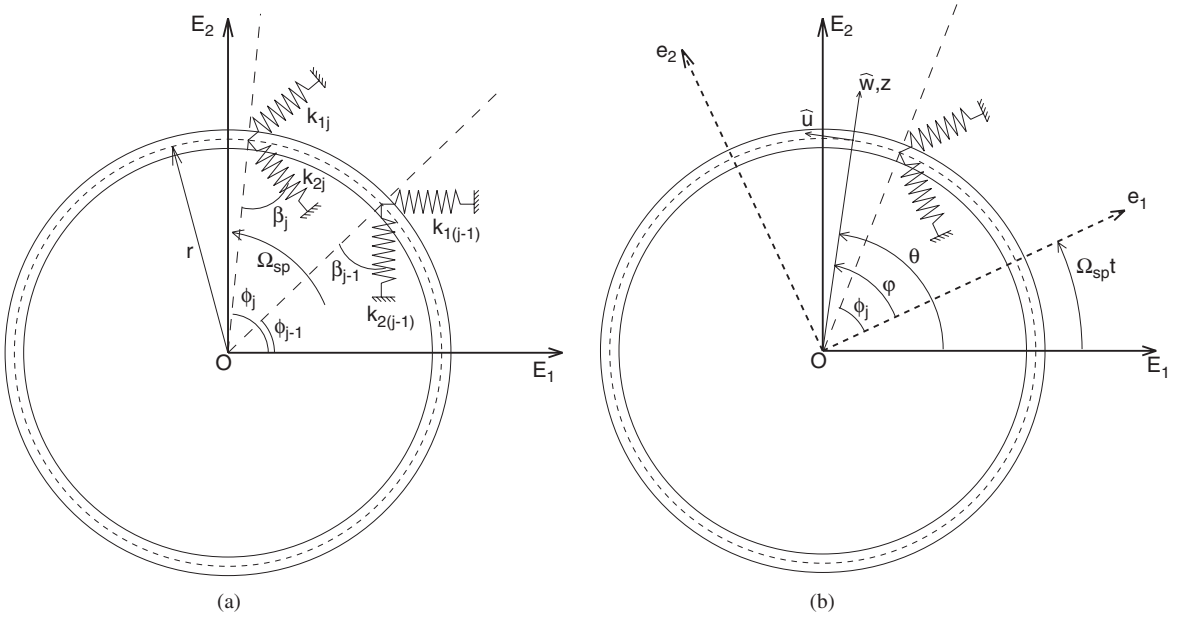

Fig. 1. (a) Schematic of a rotating ring on multiple rotating spring-sets. (b) Definition of reference frames.

most general case of discrete spring forces on a stationary ring. The spring-sets rotate around the ring with a constant angular speed Ω_{sp}. As they rotate, the orientation angles β_j and the relative angular spacing $(\phi_j - \phi_{j-1})$ between any two adjacent spring-sets do not change. Referring to Fig. 1(b), θ is the angular coordinate of any point on the ring in the inertial reference frame OE_1E_2, and φ is the angular coordinate of the same point in the rotating spring-fixed reference frame Oe_1e_2. The angular coordinates of a material point on the ring are related by $\theta = \varphi + \Omega_{sp}t$.

Only in-plane bending vibrations of the ring are considered in this work. The tangential and radial displacements of a point on the centroidal axis of the ring are defined as $\hat{u}$ and $\hat{w}$, respectively. Depending on the context, they are functions of θ or φ and t. Under the assumptions that the ring is thin, plane sections remain plane, strain varies linearly in the radial direction, and the effects of Poisson's ratio on the cross-sectional area are negligible, the linear strain–displacement relations are [22–24]

$$\varepsilon_u = \varepsilon_u^0 + z\kappa, \quad \varepsilon_u^0 = \frac{1}{r}(\hat{u}' + \hat{w}), \quad \kappa = \frac{(\hat{u}' - \hat{w}'')}{r^2}, \tag{1}$$

where ε_u^0 is the circumferential strain at the centroidal surface and z is measured positive outward from the centroidal surface; κ is the curvature change due to bending; and prime represents derivative with respect to θ. In Eq. (1), geometric nonlinearity is neglected as it is important for linear deformation of rings only in the presence of initial stress fields, like those arising due to ring rotation or static loading [25]. The strain energy of the ring is $U = \int_0^{2\pi}\int_A \frac{1}{2}E\varepsilon_u^2\, r\mathrm{d}A\,\mathrm{d}\theta$, where ε_u is the extensional circumferential strain, E is the Young's modulus of the ring, and A is the cross-sectional area. The spring strain energy is

$$V = \int_0^{2\pi} \sum_{j=1}^{M} \frac{1}{2}\left[k_{1j}(\hat{u}\cos\beta_j - \hat{w}\sin\beta_j)^2 + k_{2j}(\hat{u}\sin\beta_j + \hat{w}\cos\beta_j)^2\right]\delta(\theta - (\Omega_{sp}t + \phi_j - 2\hat{n}_j\pi))\,\mathrm{d}\theta,$$

where Dirac's delta function $\delta(\cdot)$ specifies the angular locations of the rotating spring-sets and $\hat{n}_j$ is an integer (henceforth omitted) chosen such that $0 \leqslant \theta < 2\pi$. The kinetic energy $T = (\rho A/2)\int_0^{2\pi}(\dot{\hat{u}}^2 + \dot{\hat{w}}^2)\, r\mathrm{d}\theta$, is assumed due to translational velocities alone, and rotatory inertia is neglected for a thin ring. ρ is the density. Hamilton's principle yields the coupled equations of motion

$$\begin{aligned}&\rho rA\ddot{\hat{u}} - \frac{EA}{r}(\hat{u}'' + \hat{w}') - \frac{EI}{r^3}(\hat{u}'' - \hat{w}^{IV})\\ &\quad + \sum_{j=1}^{M}\left[\delta(\theta - \Omega_{sp}t - \phi_j)\left(k_{1j}\hat{u}\cos^2\beta_j + k_{2j}\hat{u}\sin^2\beta_j + (k_{2j} - k_{1j})\hat{w}\cos\beta_j\sin\beta_j\right)\right] = 0,\end{aligned} \tag{2}$$

$$\begin{aligned}&\rho rA\ddot{\hat{w}} + \frac{EA}{r}(\hat{u}' + \hat{w}) - \frac{EI}{r^3}(\hat{u}''' - \hat{w}^{IV})\\ &\quad + \sum_{j=1}^{M}\left[\delta(\theta - \Omega_{sp}t - \phi_j)\left(k_{1j}\hat{w}\cos^2\beta_j + k_{2j}\hat{w}\sin^2\beta_j + (k_{2j} - k_{1j})\hat{u}\cos\beta_j\sin\beta_j\right)\right] = 0,\end{aligned} \tag{3}$$

where I is the moment of inertia of the ring cross-section.

Inextensibility of the centroidal axis of the ring is assumed in this work. This assumption has been used extensively in earlier research on the bending vibration of thin as well as thick rings, and the following results are available in literature. The extensibility of the centroidal surface is shown to have negligible effect on the bending natural frequencies after comparing the results with and without the inextensibility assumption to experimental results [6,8–10]. For thin rings, the primary effect of extensibility is to generate an additional set of high frequency (extensional) modes with negligible effect on the lower frequency (bending) modes [6,13]. This work investigates the in-plane bending of thin rings, and hence the inextensible centroidal surface assumption is justified. In this case $\varepsilon_u^0 = 0$ and $\hat{u}$ and $\hat{w}$ are related by $\hat{u}' + \hat{w} = 0$. The coupled Eqs. (2) and (3)

reduce to one equation for $\hat{u}$ given in non-dimensional form by

$$\frac{\partial^2}{\partial\tau^2}(u-u'')-(u^{VI}+2u^{IV}+u'')+2\pi\varepsilon\left[\sum_{j=1}^{M}\left\{(c_{1j}u+c_{2j}u')\delta(\theta-v_{sp}\tau-\phi_j)\right\}\right.$$
$$\left.-\frac{\partial}{\partial\theta}\sum_{j=1}^{M}\left\{(c_{3j}u+c_{4j}u')\delta(\theta-v_{sp}\tau-\phi_j)\right\}\right]=0, \tag{4}$$

where the dimensionless quantities are

$$u=\frac{\hat{u}}{r},\quad \tau=\omega t,\quad \omega^2=\frac{EI}{\rho Ar^4},\quad v_{sp}=\frac{\Omega_{sp}}{\omega},\quad \varepsilon=\frac{k}{2\pi k_b}$$
$$k_b=EI/r^3,\quad k=\max(k_{1j},k_{2j}),\quad j=1,2,\ldots,M,$$
$$c_{1j}=\frac{1}{k}(k_{1j}\cos^2\beta_j+k_{2j}\sin^2\beta_j),\quad c_{2j}=c_{3j}=\frac{1}{k}(k_{1j}-k_{2j})\cos\,\beta_j\,\sin\,\beta_j$$
$$c_{4j}=\frac{1}{k}(k_{1j}\sin^2\beta_j+k_{2j}\cos^2\beta_j). \tag{5}$$

The important non-dimensional parameters are ε, which represents the ratio of the stiffness of the spring-sets to the bending stiffness k_b of the ring, and the non-dimensional spring rotation speed v_{sp}. The time-varying spring forces parametrically excite the system as the angular locations of the spring-sets changes periodically. Parametric instabilities occur for particular values of the magnitude (ε) and frequency (v_{sp}) of the time-varying excitation. If the stiffness of all the springs are of the same order and small compared to the bending stiffness of the ring, then $c_{1j},c_{2j},c_{3j},c_{4j}$ are of order unity, and ε is a small quantity. Under these assumptions, perturbation methods are used to obtain closed-form approximations for the regions of parametric instability in the v_{sp}–ε plane.

3. Parametric instability analysis

To capture principal and combination instabilities, a two-term Galerkin discretization is applied to Eq. (4) using the expansion

$$u(\theta,\tau)=\psi_n(\tau)e^{in\theta}+\psi_m(\tau)e^{im\theta}+cc,\quad n,m\geqslant 2, \tag{6}$$

where cc represents the complex conjugate of all preceding terms. The restriction $n,m\geqslant 2$ eliminates rigid body motion. Defining the inner product as $\langle a,b\rangle=\int_0^{2\pi}a\bar{b}\,d\theta$, substituting Eq. (6) into Eq. (4), and forming the inner product of the resulting equation with each of the basis functions yields the coupled equations

$$\frac{d^2\psi_n}{d\tau^2}+p_n^2\psi_n+\varepsilon q_n\{G_{nn}\psi_n+H_{nn}e^{-i2nv_{sp}\tau}\overline{\psi}_n+G_{nm}e^{i(m-n)v_{sp}\tau}\psi_m+H_{nm}e^{-i(m+n)v_{sp}\tau}\overline{\psi}_m\}=0,$$
$$\frac{d^2\psi_m}{d\tau^2}+p_m^2\psi_m+\varepsilon q_m\{G_{mm}\psi_m+H_{mm}e^{-i2mv_{sp}\tau}\overline{\psi}_m+G_{mn}e^{-i(m-n)v_{sp}\tau}\psi_n+H_{mn}e^{-i(m+n)v_{sp}\tau}\overline{\psi}_n\}=0. \tag{7}$$

$$G_{nm}=\sum_{j=1}^{M}\left[\varsigma_{nm}^j+i\xi_{nm}^j\right]e^{i(m-n)\phi_j}=\sum_{j=1}^{M}\left[(c_{1j}+nmc_{4j})+i(mc_{2j}-nc_{3j})\right]e^{i(m-n)\phi_j},$$
$$H_{nm}=\sum_{j=1}^{M}\left[\gamma_{nm}^j+i\lambda_{nm}^j\right]e^{-i(m+n)\phi_j}=\sum_{j=1}^{M}\left[(c_{1j}-nmc_{4j})+i(-mc_{2j}-nc_{3j})\right]e^{-i(m+n)\phi_j}, \tag{8}$$

$$p_n^2=\frac{n^2(n^2-1)^2}{1+n^2},\qquad q_n=\frac{1}{1+n^2}.$$

G_{nm} and H_{nm} depend on the spring-set parameters, and p_n represents the non-dimensional natural frequency for the bending vibrations of a free ring in the n nodal diameter mode ($e^{\pm in\theta}$). In conjunction with Eq. (5) the

following relations involving expressions (8) hold

$$\varsigma^j_{nm} = \varsigma^j_{mn} = \varsigma^j, \quad \xi^j_{nm} = -\xi^j_{mn} = \xi^j; \xi^j_{nn} = \xi^j_{mm} = 0, \quad \gamma^j_{nm} = \gamma^j_{mn} = \gamma^j, \quad \lambda^j_{nm} = \lambda^j_{mn} = \lambda^j.$$

Although the only excitation frequency in Eq. (4) is v_{sp}, Galerkin discretization to the modal coordinates in Eq. (7) results in the two excitation frequencies $(m+n)v_{sp}$ and $(m-n)v_{sp}$, where $m \geqslant n$ is assumed without loss of generality. The spring-set force on the ring depends on the deflected shape of the ring (determined by m, n) and the location of the spring-sets (determined by v_{sp}). The $O(\varepsilon)$ terms in Eq. (7) arise from the projection onto the m nodal diameter mode of the force the rotating springs exert when the ring deflects in the n nodal diameter mode. Such a projection results in forces varying with the modulated frequencies $(m+n)v_{sp}$ and $(m-n)v_{sp}$. Therefore, the system (7) may be viewed as having two different excitation frequencies $(m+n)v_{sp}$ and $(m-n)v_{sp}$.

3.1. Conditions of parametric instability

Parametric instabilities arise when the non-dimensional spring rotation speed v_{sp} is close to particular combinations of the free ring natural frequencies p_m and p_n. The method of multiple scales applied to the coupled equations (7) identifies these instabilities. With the definitions $\tau_0 = \tau, \tau_1 = \varepsilon\tau$ for the different time scales and derivatives with respect to each denoted as $D_x = \partial/\partial\tau_x, x = 0, 1$, the time derivatives in Eq. (7) transform to $\mathrm{d}/\mathrm{d}\tau \to D_0 + \varepsilon D_1$ and $\mathrm{d}^2/\mathrm{d}\tau^2 \to D_0^2 + 2\varepsilon D_1 D_0 + O(\varepsilon^2)$. The solution is written as

$$\psi_n = \psi_{n_0}(\tau_0, \tau_1) + \varepsilon\psi_{n_1}(\tau_0, \tau_1), \qquad \psi_m = \psi_{m_0}(\tau_0, \tau_1) + \varepsilon\psi_{m_1}(\tau_0, \tau_1) \tag{9}$$

Substituting Eq. (9) into Eq. (7) and grouping terms of the same order in ε gives

$$D_0^2\psi_{n_0} + p_n^2\psi_{n_0} = 0, \qquad D_0^2\psi_{m_0} + p_m^2\psi_{m_0} = 0, \tag{10}$$

$$\begin{aligned} D_0^2\psi_{n_1} + p_n^2\psi_{n_1} = & -2D_0D_1\psi_{n_0} - q_n(G_{nn}\psi_{n_0} + H_{nn}\mathrm{e}^{-\mathrm{i}2nv_{sp}\tau_0}\overline{\psi}_{n_0} \\ & + G_{nm}\mathrm{e}^{\mathrm{i}(m-n)v_{sp}\tau_0}\psi_{m_0} + H_{nm}\mathrm{e}^{-\mathrm{i}(m+n)v_{sp}\tau_0}\overline{\psi}_{m_0}), \\ D_0^2\psi_{m_1} + p_m^2\psi_{m_1} = & -2D_0D_1\psi_{m_0} - q_m(G_{mm}\psi_{m_0} + H_{mm}\mathrm{e}^{-\mathrm{i}2mv_{sp}\tau_0}\overline{\psi}_{m_0} \\ & + G_{mn}\mathrm{e}^{-\mathrm{i}(m-n)v_{sp}\tau_0}\psi_{n_0} + H_{mn}\mathrm{e}^{-\mathrm{i}(m+n)v_{sp}\tau_0}\overline{\psi}_{n_0}). \end{aligned} \tag{11}$$

The solution to Eqs. (10) is

$$\psi_{n_0} = A_n(\tau_1)\mathrm{e}^{\mathrm{i}p_n\tau_0} + B_n(\tau_1)\mathrm{e}^{-\mathrm{i}p_n\tau_0}, \qquad \psi_{m_0} = A_m(\tau_1)\mathrm{e}^{\mathrm{i}p_m\tau_0} + B_m(\tau_1)\mathrm{e}^{-\mathrm{i}p_m\tau_0}, \tag{12}$$

where $A_{n,m}(\tau_1), B_{n,m}(\tau_1)$ are complex quantities. Insertion of Eqs. (12) into Eqs. (11) gives

$$\begin{aligned} D_0^2\psi_{n_1} + p_n^2\psi_{n_1} = & \{-\mathrm{i}2p_nD_1A_n - q_nG_{nn}A_n\}\mathrm{e}^{\mathrm{i}p_n\tau_0} - q_nH_{nn}\overline{A}_n\mathrm{e}^{-\mathrm{i}[2nv_{sp}+p_n]\tau_0} \\ & - q_nG_{nm}A_m\mathrm{e}^{\mathrm{i}[(m-n)v_{sp}+p_m]\tau_0} - q_nH_{nm}\overline{A}_m\mathrm{e}^{-\mathrm{i}[(m+n)v_{sp}+p_m]\tau_0} \\ & + \{\mathrm{i}2p_nD_1B_n - q_nG_{nn}B_n\}\mathrm{e}^{-\mathrm{i}p_n\tau_0} - q_nH_{nn}\overline{B}_n\mathrm{e}^{-\mathrm{i}[2nv_{sp}-p_n]\tau_0} \\ & - q_nG_{nm}B_m\mathrm{e}^{\mathrm{i}[(m-n)v_{sp}-p_m]\tau_0} - q_nH_{nm}\overline{B}_m\mathrm{e}^{-\mathrm{i}[(m+n)v_{sp}-p_m]\tau_0}, \end{aligned} \tag{13}$$

$$\begin{aligned} D_0^2\psi_{m_1} + p_m^2\psi_{m_1} = & \{-\mathrm{i}2p_mD_1A_m - q_mG_{mm}A_m\}\mathrm{e}^{\mathrm{i}p_m\tau_0} - q_mH_{mm}\overline{A}_m\mathrm{e}^{-\mathrm{i}[2mv_{sp}+p_m]\tau_0} \\ & - q_mG_{mn}A_n\mathrm{e}^{\mathrm{i}[(n-m)v_{sp}+p_n]\tau_0} - q_mH_{mn}\overline{A}_m\mathrm{e}^{-\mathrm{i}[(m+n)v_{sp}+p_n]\tau_0} \\ & + \{\mathrm{i}2p_mD_1B_m - q_mG_{mm}B_m\}\mathrm{e}^{-\mathrm{i}p_m\tau_0} - q_mH_{mm}\overline{B}_m\mathrm{e}^{-\mathrm{i}[2mv_{sp}-p_m]\tau_0} \\ & - q_mG_{mn}B_n\mathrm{e}^{\mathrm{i}[(n-m)v_{sp}-p_n]\tau_0} - q_mH_{mn}\overline{B}_n\mathrm{e}^{-\mathrm{i}[(m+n)v_{sp}-p_n]\tau_0}. \end{aligned} \tag{14}$$

Terms leading to resonant response (secular terms) may arise in Eqs. (13) and (14) when

$$(m \pm n)v_{sp} \approx p_m + p_n, \tag{15}$$

which are summation type combination instabilities of the first (plus sign: $m+n$) and second (minus sign: $m-n$) kind, or when

$$(m \pm n)v_{sp} \approx p_m - p_n, \tag{16}$$

which are difference type combination instabilities of the first and second kind. The principal instability corresponding to the nth mode is obtained from Eq. (15) with $m=n$, giving

$$nv_{sp} \approx p_n. \tag{17}$$

In arriving at Eqs. (15) and (16), $m \geqslant n$ and $v_{sp} \geqslant 0$ are assumed without loss of generality.

Combination instabilities of two kinds occur in the system because there are two related excitation frequencies $(m+n)v_{sp}$ and $(m-n)v_{sp}$. Corresponding to each of these excitation frequencies, there is a possible summation or difference type instability. In other words, there are two values of v_{sp} that can potentially result in a summation or difference type combination instability for any two modes.

3.2. Instability boundaries

The parametric instability when $(m+n)v_{sp} \approx p_m + p_n$ is considered. Let

$$(m+n)v_{sp} = p_m + p_n + \varepsilon\,\hat{\sigma}, \tag{18}$$

where $\hat{\sigma}$ is the detuning parameter. From Floquet theory, periodic solutions separate the stable and unstable regions in a parameter space. Substitution of Eq. (18) into Eqs. (13) and (14) and elimination of terms leading to unbounded, aperiodic response yields the solvability conditions

$$\begin{aligned} &\mathrm{i}2p_n D_1 B_n - q_n G_{nn} B_n - q_n \overline{B}_m H_{nm} \mathrm{e}^{-\mathrm{i}\hat{\sigma}\tau_1} = 0, \\ &\mathrm{i}2p_m D_1 B_m - q_m G_{mm} B_m - q_m \overline{B}_n H_{mn} \mathrm{e}^{-\mathrm{i}\hat{\sigma}\tau_1} = 0. \end{aligned} \tag{19}$$

With the substitutions $B_n(\tau_1) = x_n(\tau_1)\mathrm{e}^{\mathrm{i}y_n(\tau_1)}$, $B_m(\tau_1) = x_m(\tau_1)\mathrm{e}^{\mathrm{i}y_m(\tau_1)}$, where x_n, y_n, x_m, y_m are real quantities, non-trivial solutions to Eqs. (19) occur when

$$\begin{aligned} &\hat{\sigma} = \frac{q_n}{2p_n}\sum_{j=1}^{M}\xi_{nn}^j + \frac{q_m}{2p_m}\sum_{j=1}^{M}\xi_{mm}^j \pm \sqrt{\frac{q_n q_m \hat{\Delta}}{p_n p_m}}, \qquad \hat{\Delta} = \hat{I}^2 + \hat{R}^2, \\ &\hat{I} = \sum_{j=1}^{M}(\lambda^j \cos\hat{\mu}_j - \gamma^j \sin\hat{\mu}_j), \quad \hat{R} = \sum_{j=1}^{M}(\gamma^j \cos\hat{\mu}_j + \lambda^j \sin\hat{\mu}_j), \quad \hat{\mu}_j = (m+n)\phi_j. \end{aligned} \tag{20}$$

Hence, summation combination instability boundaries of the first kind are given by

$$v_{sp} = \frac{(p_m + p_n) + \varepsilon\hat{\sigma}}{(m+n)}. \tag{21}$$

The nth mode principal instability boundaries are given by $v_{sp} = (2p_n + \varepsilon\hat{\sigma})/2n$.

Turning to the parametric instability when $(m-n)v_{sp} \approx p_m + p_n$, let

$$(m-n)v_{sp} = p_m + p_n + \varepsilon\,\tilde{\sigma}. \tag{22}$$

Substitution of Eq. (22) into Eqs. (13) and (14) gives the conditions for elimination of secular terms

$$\begin{aligned} &-\mathrm{i}2p_n D_1 A_n - q_n G_{nn} A_n - q_n B_m G_{nm} \mathrm{e}^{\mathrm{i}\tilde{\sigma}\,\tau_1} = 0, \\ &\mathrm{i}2p_m D_1 B_m - q_m G_{mm} B_m - q_m A_n G_{mn} \mathrm{e}^{-\mathrm{i}\tilde{\sigma}\,\tau_1} = 0. \end{aligned} \tag{23}$$

Proceeding as in Eqs. (19)–(21), the summation combination instability boundaries of the second kind are

$$v_{sp} = \frac{(p_m + p_n) + \varepsilon\,\tilde{\sigma}}{(m-n)},$$

$$\tilde{\sigma} = \frac{q_n}{2p_n}\sum_{j=1}^{M}\varsigma_{nn}^{j} + \frac{q_m}{2p_m}\sum_{j=1}^{M}\varsigma_{mm}^{j} \pm \sqrt{\frac{q_n q_m \tilde{\Delta}}{p_n p_m}},\ \tilde{\Delta} = \tilde{I}^2 + \tilde{R}^2,$$

$$\tilde{I} = \sum_{j=1}^{M}(\varsigma^j \cos\tilde{\mu}_j + \xi^j \sin\tilde{\mu}_j), \qquad \tilde{R} = \sum_{j=1}^{M}(\varsigma^j \cos\tilde{\mu}_j - \xi^j \sin\tilde{\mu}_j), \qquad \tilde{\mu}_j = (m-n)\phi_j. \tag{24}$$

It can be shown mathematically that difference type instabilities cannot occur when $(m \pm n)v_{sp} \approx p_m - p_n$ because such a condition yields complex solutions for the detuning parameter.

The full range of possible parametric instability regions for a stationary ring with multiple discrete rotating spring-sets is captured in Eqs. (21) and (24) as relations in the spring rotation speed v_{sp} and the spring to ring bending stiffness ratio ε.

4. Numerical solution

Numerical verification of the analytical solution is performed using two approaches. In the first method, Galerkin discretization of Eq. (4) with basis functions as $e^{\pm in\theta}$ yields a time-varying state matrix form $\dot{\mathbf{x}}(\tau) = \mathbf{P}(\tau)\mathbf{x}(\tau)$ with period $T = 2\pi/v_{sp}$. Applying Floquet's theorem, the monodromy matrix $\mathbf{E}$ for the system is constructed by time integration over one period, and the eigenvalues of $\mathbf{E}$ dictate the stability of the system. By computing the monodromy matrix eigenvalues for a range of ε and v_{sp}, the regions of instability are obtained in the v_{sp}–ε parameter plane. This method is computationally intensive because of the numerical time integration, especially for small v_{sp} and so long period T.

Alternatively, the system can be analyzed in a spring-fixed reference frame, allowing much more computationally efficient evaluation of system stability. The equation of motion in the spring-fixed reference frame is obtained using the transformation $\varphi = \theta - v_{sp}\tau$ as

$$\left(\frac{\partial}{\partial\tau} - v_{sp}\frac{\partial}{\partial\varphi}\right)^2 (u - u'') - (u^{VI} + 2u^{IV} + u'') + 2\pi\varepsilon\left[\sum_{j=1}^{M}\left\{(c_{1j}u + c_{2j}u')\delta(\varphi - \phi_j)\right\}\right.$$
$$\left. - \frac{\partial}{\partial\varphi}\sum_{j=1}^{M}\left\{(c_{3j}u + c_{4j}u')\delta(\varphi - \phi_j)\right\}\right] = 0, \tag{25}$$

where prime denotes partial derivative with respect to φ. In this reference frame, the angular locations of the spring-sets do not change with time, and Eq. (25) is not a parametrically excited system. Instead, the self-adjoint system in Eq. (4) changes to a gyroscopic one as a result of the term $-2v_{sp}\partial(u' - u''')/\partial\tau$, which has a skew-self adjoint spatial operator. Galerkin discretization of Eq. (25) with basis functions $e^{\pm in\varphi}$ now yields a time-invariant state matrix form $\dot{\mathbf{x}}(\tau) = \mathbf{Q}\,\mathbf{x}(\tau)$. The stability of the system is dictated by whether or not an eigenvalue of $\mathbf{Q}$ has a positive real part. By computing $\mathbf{Q}$ and its eigenvalues for ranges of ε and v_{sp} (or other parameters), the regions of instability are obtained.

5. Results and discussion

The analytical and numerical results for the stability boundaries are plotted in the v_{sp}–ε plane. Fig. 2 shows these results for the case of one radial rotating spring. The analytical stability boundaries are obtained using Eqs. (20), (21) and (24). Only the first three bending modes, namely, modes with 2, 3 and 4 nodal diameters are considered. The numerical instability regions are also computed taking the first three modes (starting with $n = 2$) to discretize the tangential displacement in Eqs. (4) and (25). The agreement between the analytical and numerical results is evident, even for relatively large values of the spring stiffness to bending stiffness ratio ε. Both numerical methods were used to verify the analytical results, and they yield the same instability regions.

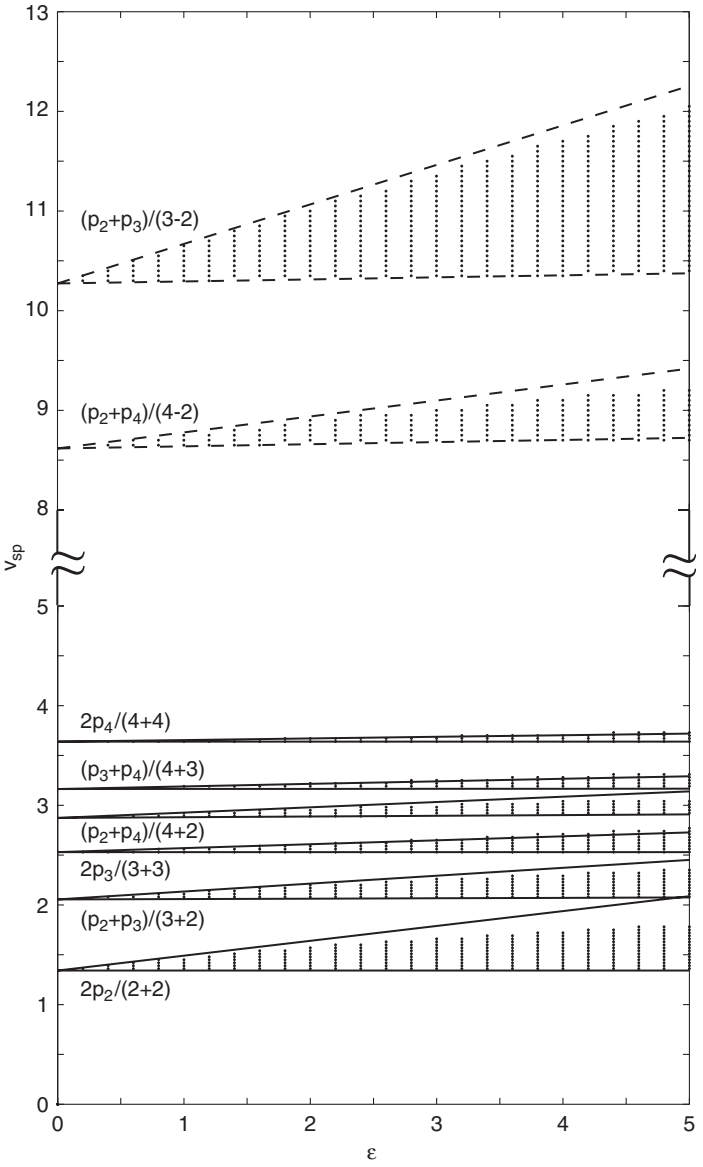

Fig. 2. Parametric instability regions for one radial rotating spring with $k_{11} = 0$, $k_{21} = k$, $\beta_1 = 0^\circ$. —, principal and combination instabilities of first kind; - - -, combination instabilities of second kind; ⁂, numerical solution.

The convergence of the numerical results is verified in Fig. 3. The real and imaginary parts of the eigenvalues of **Q** are shown for $\varepsilon = 1$. Parametric instabilities occur when the real part of an eigenvalue becomes positive. From Fig. 3(a), a one-term approximation captures principal instability due to that mode. The width of the instability region in Fig. 2 when $\varepsilon = 1$ corresponds well with the width of the region where the real part is positive in Fig. 3(a). A two-term approximation captures principal and combination instabilities that arise from the two modes under consideration (Fig. 3(a)). Increasing the number of terms does not significantly change the width of the unstable regions obtained using fewer terms (Fig. 3(b)), but new principal and combination instabilities appear corresponding to the additional modes in the discretization. To compare the analytical results that arise from the first n nodal diameter bending modes, an approximation with n terms in the numerical scheme is sufficiently accurate. The analytical results presented here show instabilities arising

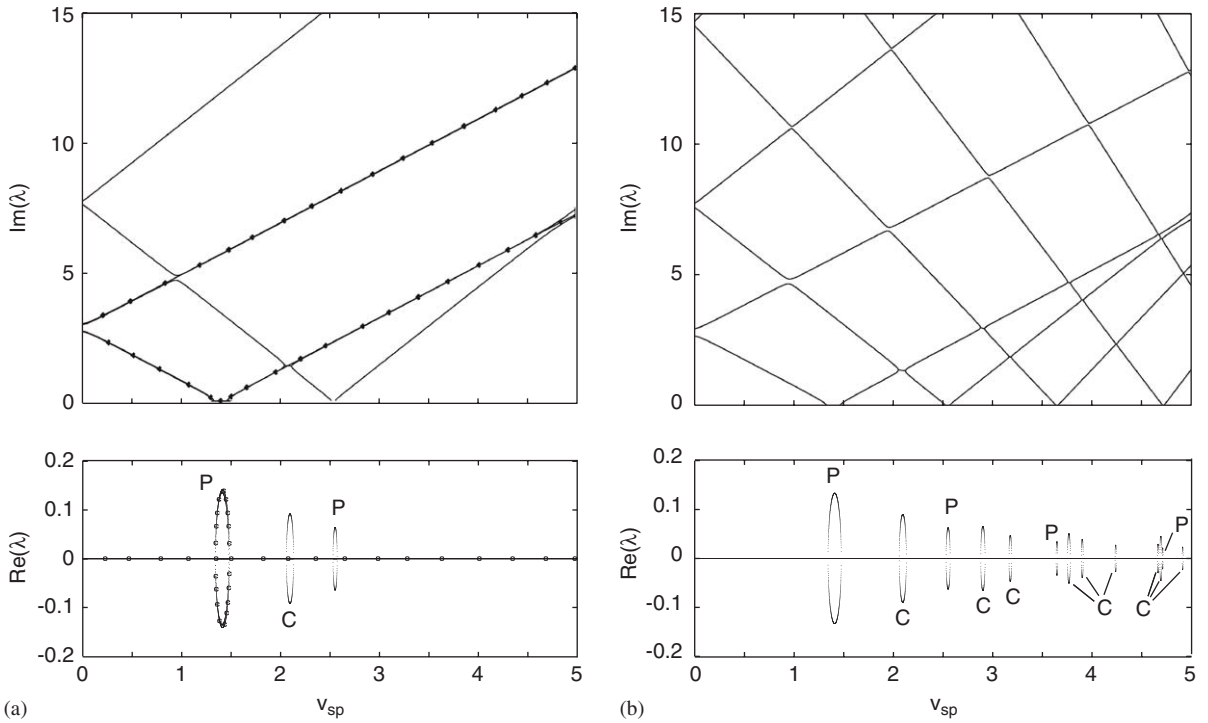

Fig. 3. Real and imaginary parts of the eigenvalues of matrix $\mathbf{Q}$ with one radial rotating spring with $\varepsilon = k/2\pi k_b = 1$, $k_{11} = 0$, $k_{21} = k$, $\beta_1 = 0^\circ$. P: principal instability, C: combination instability. (a) $-\bullet-$, one-term approximation; —, two-term approximation. (b) Ten-term approximation.

from the first three bending modes (2, 3 and 4 nodal diameters), and these are compared against numerical results using the first three terms for approximation.

Fig. 3 gives additional information on the nature of instability as observed from the spring-fixed reference frame. The real parts of the eigenvalues become positive (unstable) when two imaginary eigenvalues coalesce. If the imaginary eigenvalues coalesce at zero, divergence instability occurs, and if they coalesce at a non-zero value, flutter instability occurs. Principal instabilities are always of the divergence kind, and combination instabilities are of the flutter kind.

5.1. Effect of number of spring-sets, symmetry and asymmetry

The width of the parametric instability regions are governed by $\hat{\Delta}$ and $\tilde{\Delta}$ defined in Eqs. (20) and (24). Their values depend on the parameters of the spring-sets, namely, the number of spring-sets, the stiffness of the individual springs, their orientation and their spacing. Symmetry is common in physical systems and is often exploited. In many cases, symmetry has inherent advantages, including in planetary gears. It is interesting as well as useful to study how symmetry affects the parametric instabilities.

Parametric instability regions appear only if $\hat{\Delta}$ or $\tilde{\Delta}$ are non-zero. When all the spring-sets are identical with the same individual spring stiffnesses and orientation angles, then $\varsigma^j = \varsigma$, $\xi^j = \xi$, $\gamma^j = \gamma$, and $\lambda^j = \lambda$ for $j = 1, 2, ..., M$. In this case,

$$\hat{\Delta} = (\gamma^2 + \lambda^2)\left\{\left[\sum_{j=1}^{M} \cos(m+n)\phi_j\right]^2 + \left[\sum_{j=1}^{M} \sin(m+n)\phi_j\right]^2\right\}, \tag{26}$$

$$\tilde{\Delta} = (\varsigma^2 + \xi^2)\left\{\left[\sum_{j=1}^{M}\cos(m-n)\phi_j\right]^2 + \left[\sum_{j=1}^{M}\sin(m-n)\phi_j\right]^2\right\}. \tag{27}$$

If, in addition, the spring-sets are equally spaced, then

$$\phi_j = \frac{2\pi(j-1)}{M}, \qquad j = 1, 2, ..., M. \tag{28}$$

The following trigonometric identities hold for integer values of s

$$\sum_{j=1}^{M}\sin\left[\frac{2\pi(j-1)s}{M}\right] = 0, \qquad \sum_{j=1}^{M}\cos\left[\frac{2\pi(j-1)s}{M}\right] = \begin{cases} 0, & s/M \neq \text{integer}, \\ M, & s/M = \text{integer}. \end{cases} \tag{29}$$

Use of Eqs. (28) and (29) in Eqs. (26) and (27) yields that $\hat{\Delta}$ is non-zero only when the nodal diameters m and n are related to the total number of spring-sets M by

$$m + n = sM, \qquad s = 1, 2, 3, ... \tag{30}$$

$\tilde{\Delta}$ is non-zero only when

$$m - n = sM, \qquad s = 1, 2, 3, ... \tag{31}$$

For the case of identical and equally spaced spring-sets (referred to as the symmetric case), symmetry of the system suppresses certain parametric instabilities (many, in fact), both principal and combination. Principal and combination instabilities of the first kind appear only for those modes whose nodal diameters satisfy Eq. (30), and combination instabilities of the second kind appear only for those modes whose nodal diameters satisfy Eq. (31).

To illustrate these results, examples with two and three radial springs are presented considering the 2, 3 and 4 nodal diameter modes. For two radial rotating springs, Fig. 4(a) shows the instabilities for the symmetric case. In comparison to the asymmetric case (identical, unequally spaced spring-sets) in Fig. 4(b), some instabilities are suppressed by symmetry. In fact, the only instabilities that appear in the symmetric case are principal instabilities of the 2, 3 and 4 nodal diameter modes, and summation combination instability (first and second kinds) due to interaction of the 2 and 4 nodal diameter modes. These results verify the predictions in Eqs. (30) and (31). Similarly, considering the case of three radial springs, the only instabilities that appear in the symmetric case (Fig. 5(a)) are the principal instability due to the three nodal diameter mode, and the combination instability of the first kind from interaction of the two and four nodal diameter modes. In the asymmetric cases of identical, unequally spaced spring-sets (Fig. 5(b)), or non-identical, equally spaced spring-sets (Fig. 5(c)), all possible instabilities occur.

5.2. Parametric study

The analytical solution shows how parametric instability regions change due to a variation in the system parameters. As examples, the effects of orientation angle (β), stiffness angle (α) and modulation angle (Υ) are considered. For the case of one rotating spring ($k_{11} = 0, k_{21} = k$), the orientation angle is varied from $\beta = 0^\circ$ (radial) to $\beta = 90^\circ$ (tangential), and the result is shown in Fig. 6. Larger instability regions appear when the same spring is oriented in the radial direction versus the tangential direction. This result is verified starting with Eq. (5), which gives $c_{1j} = c_{2j} = c_{3j} = 0, c_{4j} = 1$ when $\beta = 0^\circ$, and $c_{1j} = 1, c_{2j} = c_{3j} = c_{4j} = 0$ when $\beta = 90^\circ$. Accordingly, from Eq. (8), $\xi^j = \lambda^j = 0, \varsigma^j = nm, \gamma^j = -nm$ when $\beta = 0^\circ$; and $\xi^j = \lambda^j = 0, \varsigma^j = 1, \gamma^j = 1$ when $\beta = 90^\circ$. The instability region width depends on the magnitudes of $\hat{\Delta}$ and $\tilde{\Delta}$ in Eqs. (20) and (24),

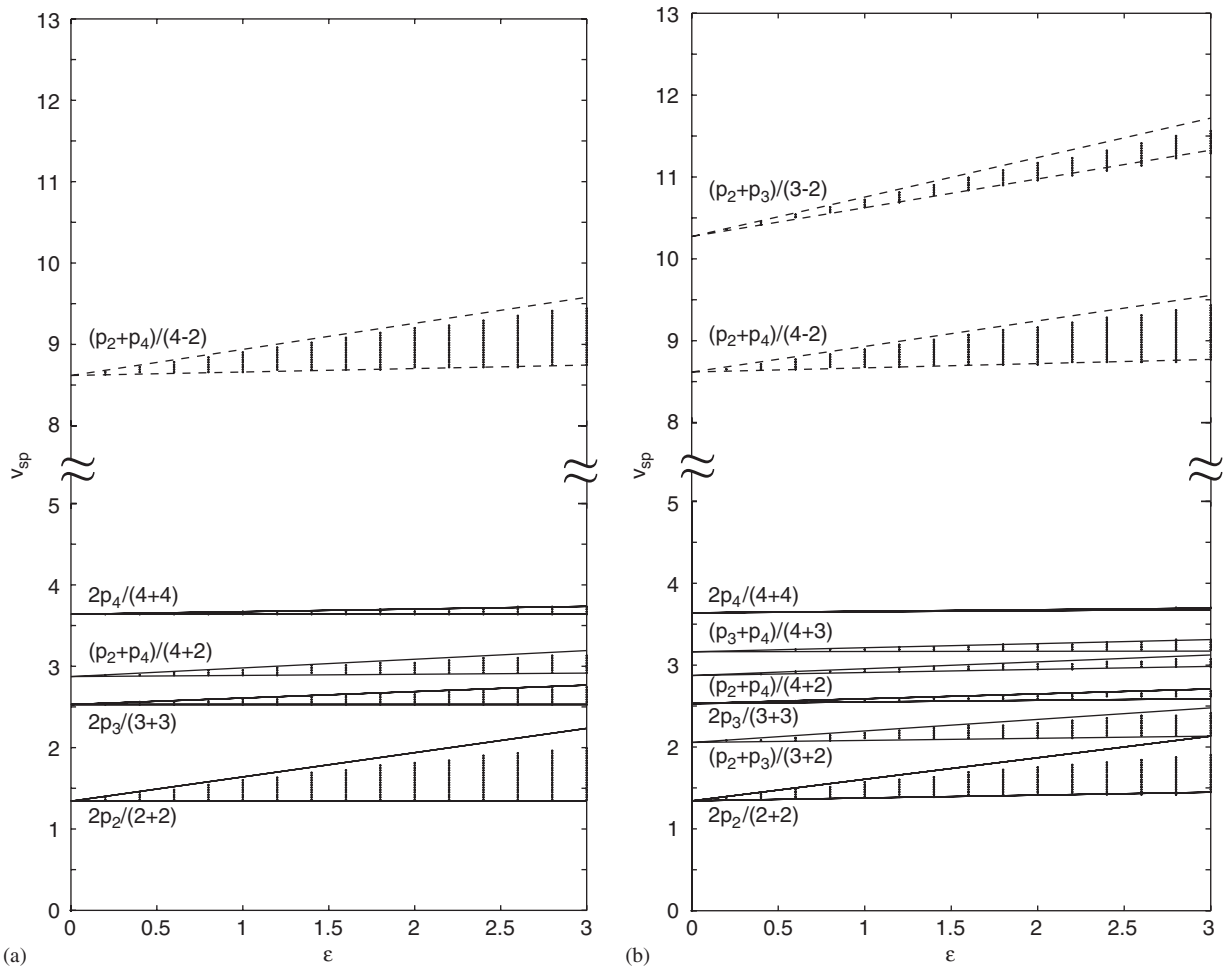

Fig. 4. Parametric instability regions for two identical rotating radial springs with $k_{1j}=0$, $k_{2j}=k$, $\beta_j=0^\circ$. (a) Symmetric case with equally spaced rotating radial springs. (b) Asymmetric case with unequally spaced rotating radial springs with $\phi_1=0^\circ, \phi_2=160^\circ$. —, principal and combination instabilities of first kind; - - -, combination instabilities of second kind; ***, numerical solution.

which simplify to

$$\hat{\Delta}=(\gamma^j)^2\left[\left(\sum_{j=1}^{M}\cos\,\hat{\mu}_j\right)^2+\left(\sum_{j=1}^{M}\sin\,\hat{\mu}_j\right)^2\right],$$
$$\tilde{\Delta}=(\varsigma^j)^2\left[\left(\sum_{j=1}^{M}\cos\,\tilde{\mu}_j\right)^2+\left(\sum_{j=1}^{M}\sin\,\tilde{\mu}_j\right)^2\right]. \tag{32}$$

Substituting values of γ^j and ς^j for tangential and radial spring orientations into Eqs. (32), recognizing that $\hat{\mu}_j$ and $\tilde{\mu}_j$ are independent of β, and utilizing $nm\geqslant 4>1$ yields that $\hat{\Delta}$ and $\tilde{\Delta}$ are both larger when $\beta=0^\circ$ (radial springs).

The stiffness angle is defined as $\alpha_j=\tan^{-1}\left(k_{2j}/k_{1j}\right)$ $(0^\circ\leqslant\alpha_j\leqslant 90^\circ)$, so that $k_{1j}=k_j\cos\alpha_j$, $k_{2j}=k_j\sin\alpha_j$ where $k_j=\sqrt{k_{1j}^2+k_{2j}^2}$. Together, k_j and α_j quantify the effective stiffness along the directions in-line and perpendicular to the axis defined by the orientation angle β_j. When $\beta_j=0^\circ$, purely tangential and purely radial

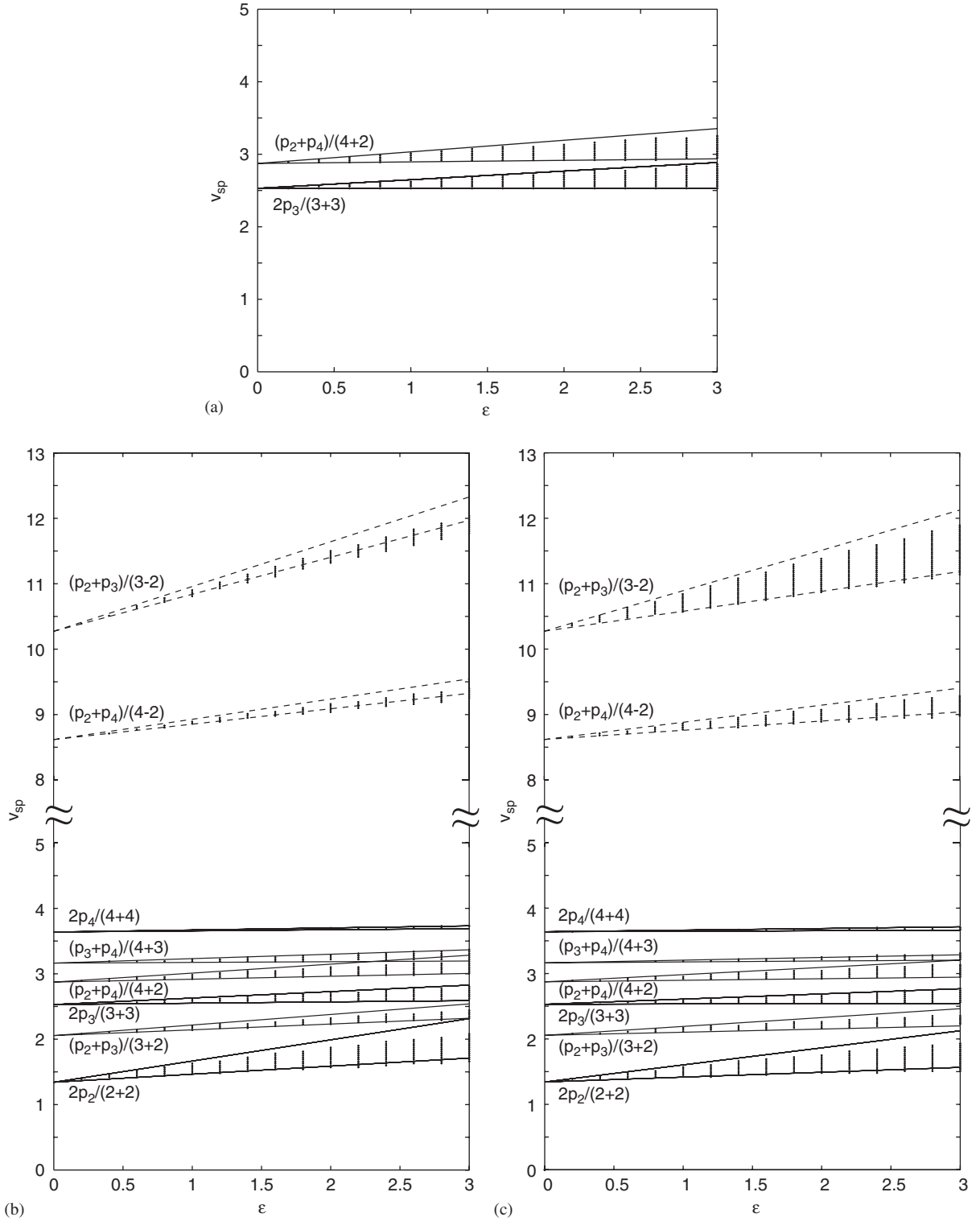

Fig. 5. Parametric instability regions. (a) Symmetric case of three identical and equally spaced rotating radial springs with $k_{1j}=0$, $k_{2j}=k$, $\beta_j=0^\circ$. Asymmetric cases: (b) Three identical but unequally spaced rotating radial springs with $k_{1j}=0$, $k_{2j}=k$, $\beta_j=0^\circ$; $\phi_1=0^\circ$, $\phi_2=110^\circ$, $\phi_3=250^\circ$. (c) Three non-identical but equally spaced rotating radial springs with $k_{21}=k_{23}=k_{12}=k$, $\beta_j=0^\circ$. —, principal and combination instabilities of first kind; - - -, combination instability of second kind; ***, numerical solution.

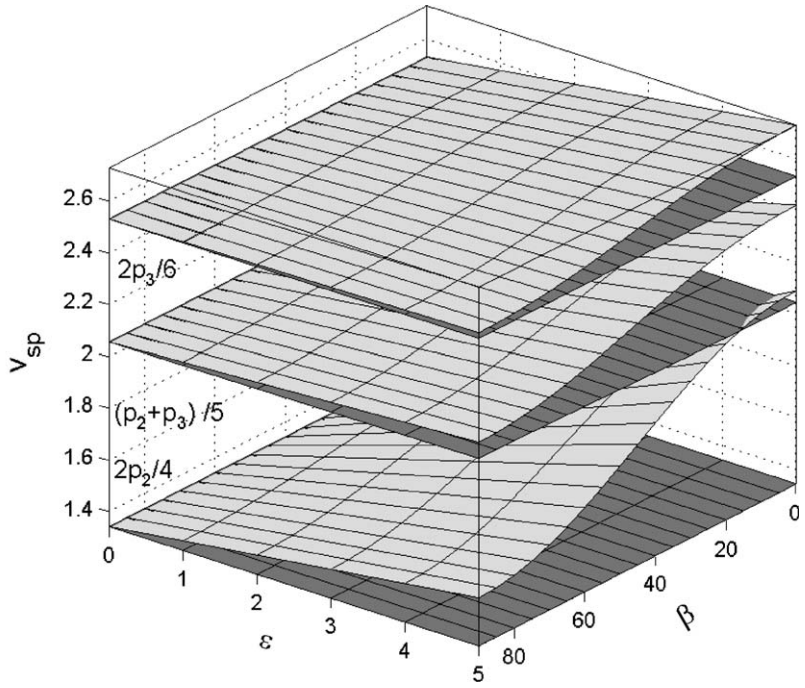

Fig. 6. Effect of spring orientation angle on parametric instability regions: one rotating spring with $k_{11} = 0, k_{21} = k$.

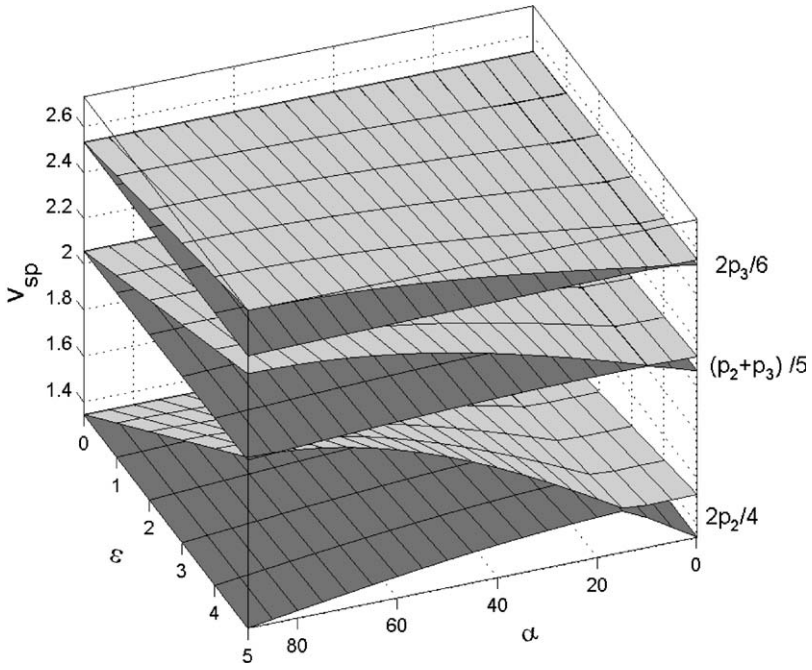

Fig. 7. Effect of stiffness angle on parametric instability regions: one rotating spring-set with $k_1 = k, \beta = 0^\circ$.

springs correspond to $\alpha_j = 0^\circ$ and 90°, respectively. Considering a single rotating spring-set defined by k, α, Fig. 7 shows the instability zones for different values of α with $\beta_j = 0^\circ$. As obtained previously, the instability regions are larger for radial orientation of the spring compared to tangential orientation. Interestingly, for

$\beta_j = 0^\circ$, the different combination instabilities of the first kind, including principal instabilities, vanish for particular values of α, as indicated in Fig. 7 by closing of the instability regions in the v_{sp}–ε plane. The analytical expressions (5), (8) and (20) show that $\lambda^j = 0$ when $\beta_j = 0^\circ$. Furthermore if all the spring-sets have the same stiffness angle $\alpha_j = \alpha$, then

$$\hat{\Delta} = \left(\sum_{j=1}^{M} \gamma^j \cos \hat{\mu}_j\right)^2 + \left(\sum_{j=1}^{M} \gamma^j \sin \hat{\mu}_j\right)^2$$
$$= \left(\frac{\cos\alpha - nm \sin\alpha}{\max(k_{1j}, k_{2j})}\right)^2 \left[\left(\sum_{j=1}^{M} k_j \cos \hat{\mu}_j\right)^2 + \left(\sum_{j=1}^{M} k_j \sin \hat{\mu}_j\right)^2\right]. \quad (33)$$

Combination instabilities of the first kind due to the n and m nodal diameter modes vanish if $\tan\alpha = 1/nm$. Consequently, principal instabilities corresponding to 2 and 3 nodal diameter modes vanish when $\alpha = 14.03^\circ$ and 6.34°, respectively, and the combination instability due to their interaction vanishes when $\alpha = 9.46^\circ$ (Fig. 7). These results hold for arbitrary spacing of spring-sets with different k_j, so long as $\beta_j = 0^\circ$, and the stiffness angles for all the spring-sets are the same. Combination instabilities of the second kind do not exhibit similar behavior because there is no value of α ($0^\circ \leqslant \alpha \leqslant 90^\circ$) for which $\tilde{\Delta} = 0$.

Consider spring-sets that are placed in diametrically opposed pairs. Such a configuration is of practical importance in planetary gear systems where equal planet spacing is not possible due to assembly requirements. They are placed in diametrically opposed pairs because of bearing force and load sharing considerations. The effect of angular spacing between the diameters on the parametric instabilities is shown in Fig. 8 for two pairs of diametrically opposed radial springs ($\varepsilon = 1$) located at $\phi_1 = 0^\circ$, $\phi_2 = 90^\circ + \Upsilon^\circ, \phi_3 = 180^\circ$ and $\phi_4 = 270^\circ + \Upsilon^\circ$, where Υ is the modulation angle. The width of the instability regions vary with the modulation angle and are plotted for the range $\Upsilon = 0^\circ$ to 90°. Some instabilities vanish entirely for diametrically opposed pairs of spring-sets. For those that appear, some instabilities vanish depending on the value of the modulation angle Υ. To explain this analytically, consider the expressions for $\hat{\Delta}$, $\tilde{\Delta}$ from Eqs. (26)

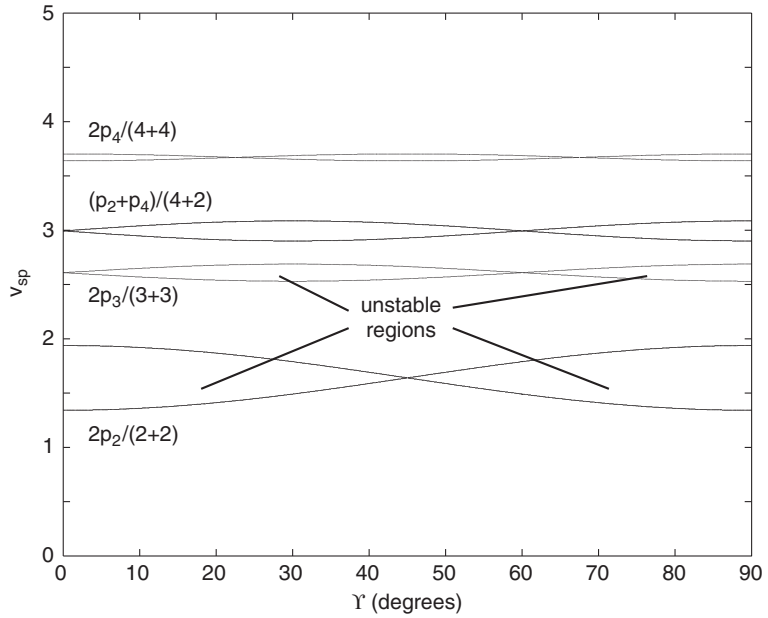

Fig. 8. Effect of modulation angle on parametric instability boundaries for two pairs of diametrically opposed radial springs with $\varepsilon = k/2\pi k_b = 1$, $k_{1j} = 0$, $k_{2j} = k$, $\beta_j = 0^\circ$; $\phi_1 = 0^\circ$, $\phi_2 = 90^\circ + \Upsilon^\circ$, $\phi_3 = 180^\circ$, $\phi_4 = 270^\circ + \Upsilon^\circ$.

and (27) for identical, diametrically opposed spring-sets

$$\hat{\Delta} = (\gamma^2+\lambda^2)\left\{\left[\sum_{j=1}^{M/2}\left(\cos\left[(m+n)\phi_j\right]+\cos\left[(m+n)\phi_j+(m+n)\pi\right]\right)\right]^2 + \left[\sum_{j=1}^{M/2}\left(\sin\left[(m+n)\phi_j\right]+\sin\left[(m+n)\phi_j+(m+n)\pi\right]\right)\right]^2\right\}$$

$$= \begin{cases} 0 & \text{if } (m+n) \text{ is odd,} \\ (\gamma^2+\lambda^2)\left\{\left[2\sum_{j=1}^{M/2}\left(\cos\left[(m+n)\phi_j\right]\right)\right]^2+\left[2\sum_{j=1}^{M/2}\left(\sin\left[(m+n)\phi_j\right]\right)\right]^2\right\}, & \text{if } (m+n) \text{ is even,} \end{cases} \tag{34}$$

$$\tilde{\Delta} = (\varsigma^2+\xi^2)\left\{\left[\sum_{j=1}^{M/2}\left(\cos\left[(m-n)\phi_j\right]+\cos\left[(m-n)\phi_j+(m-n)\pi\right]\right)\right]^2 + \left[\sum_{j=1}^{M/2}\left(\sin\left[(m-n)\phi_j\right]+\sin\left[(m+n)\phi_j+(m-n)\pi\right]\right)\right]^2\right\}$$

$$= \begin{cases} 0 & \text{if } (m-n) \text{ is odd,} \\ (\varsigma^2+\xi^2)\left\{\left[2\sum_{j=1}^{M/2}\left(\cos\left[(m-n)\phi_j\right]\right)\right]^2+\left[2\sum_{j=1}^{M/2}\left(\sin\left[(m-n)\phi_j\right]\right)\right]^2\right\} & \text{if } (m-n) \text{ is even.} \end{cases} \tag{35}$$

Hence, for identical and diametrically opposed spring-sets, parametric instabilities cannot occur if $m \pm n$ is odd. This is confirmed from Fig. 8. If $m \pm n$ is even, however, $\hat{\Delta}$ or $\tilde{\Delta}$ may become zero depending on the values of m, n, ϕ_j and M. For example, in Fig. 8, the principal instability from $n = 2$ vanishes when $\Upsilon = 45^\circ$.

5.3. Simultaneous rotating and non-rotating springs

An interesting related problem is that of a ring supported with fixed discrete spring supports simultaneously subjected to parametric excitation from multiple rotating spring-sets. Planetary gear systems in a fixed ring configuration are a good example, where the bolts that arrest the ring gear are represented by the fixed springs, and the ring-planet mesh stiffnesses are represented by the rotating spring-sets. Certain bearing races are another example.

The equation of motion for this problem is similar to Eq. (4) as given below:

$$\frac{\partial^2}{\partial\tau^2}(u-u'') - \left(u^{VI}+2u^{IV}+u''\right) + \left[\sum_{j=1}^{M}\left\{(\hat{c}_{1j}u+\hat{c}_{2j}u')\delta(\theta-\hat{\phi}_j)\right\} - \frac{\partial}{\partial\theta}\sum_{j=1}^{M}\left\{(\hat{c}_{3j}u+\hat{c}_{4j}u')\delta(\theta-\hat{\phi}_j)\right\}\right] + 2\pi\varepsilon\left[\sum_{j=1}^{M}\left\{(c_{1j}u+c_{2j}u')\delta(\theta-v_{sp}\tau-\phi_j)\right\} - \frac{\partial}{\partial\theta}\sum_{j=1}^{M}\left\{(c_{3j}u+c_{4j}u')\delta(\theta-v_{sp}\tau-\phi_j)\right\}\right] = 0, \tag{36}$$

where

$$\hat{c}_{1j} = \frac{1}{k_b}(\hat{k}_{1j}\cos^2\hat{\beta}_j + \hat{k}_{2j}\sin^2\hat{\beta}_j), \qquad \hat{c}_{2j} = \hat{c}_{3j} = \frac{1}{k_b}(\hat{k}_{1j}-\hat{k}_{2j})\cos\,\hat{\beta}_j\,\sin\,\hat{\beta}_j,$$
$$\hat{c}_{4j} = \frac{1}{k_b}(\hat{k}_{1j}\sin^2\hat{\beta}_j + \hat{k}_{2j}\cos^2\hat{\beta}_j)$$

are the fixed spring-set coefficients and $c_{1j}, c_{2j}, c_{3j}, c_{4j}$ are the rotating spring-set coefficients defined in Eq. (5). Both the fixed and rotating spring-sets represent the most general discrete spring loading, each consisting of two springs in perpendicular directions at some orientation angle. Assuming that the stiffnesses of the rotating springs are small compared to the bending stiffness of the ring and capturing this by the quantity ε as before, the problem is formulated such that $\varepsilon = 0$ represents the vibration of a ring on fixed spring supports.

The vibrations of a ring on general elastic foundation have been studied using perturbation methods, and as a special case, the natural frequencies and vibration modes of rings on discrete spring supports were obtained [12]. For a ring on M_f identical, equally spaced discrete spring-sets (called symmetric fixed spring-sets), the degenerate natural frequencies of the n nodal diameter mode split only if

$$n = \begin{cases} \dfrac{sM_f}{2}, & \text{for even } M_f \\ sM_f, & \text{for odd } M_f, \end{cases} \quad s = 1, 2, 3, \ldots \tag{37}$$

The fixed spring-sets alter the modal properties of the non-parametrically excited system ($\varepsilon = 0$) and hence affect the parametric instabilities. Closed-form analytical solutions using perturbation techniques were attempted but proved too cumbersome. The problem is investigated numerically. Because this system cannot be cast in a time-invariant form by a suitable choice of reference frame, Floquet theory is used to determine the stability of the time-varying system. As discussed previously, Galerkin discretization of Eq. (36) yields a periodic time-varying state matrix form, and the monodromy matrix eigenvalues dictate the system stability.

The 2 and 3 nodal diameter mode instabilities for a ring with one rotating radial spring and two identical, equally spaced (symmetric) fixed radial springs are shown in Fig. 9. Comparing with Fig. 2, the fixed springs cause parametric instability regions to split. A summary of key results is presented in Table 1. The first column gives the nodal diameters considered for studying parametric instabilities. The second column states whether parametric instability occurs when only rotating springs are present without fixed springs (Eqs. (30) and (31)). The third column states whether the ring natural frequencies split when only symmetric fixed springs are present without rotating ones (Eq. (37)), and the split natural frequencies are shown. The last two columns give the excitation frequencies (spring-set rotation speeds v_{sp}) around which parametric instabilities are expected to occur when rotating and fixed spring-sets are considered together. These are obtained by applying Eq. (15) to the split natural frequency modes. These values are confirmed by the results in Fig. 9 (where high

Table 1
Spring rotation speeds where parametric instability regions occur with one radial rotating spring with $k_{11} = 0$, $k_{21} = k$, $\beta_1 = 0^\circ$ and two radial symmetric fixed springs with $\hat{k}_{1j} = 0$, $\hat{k}_{2j} = 2\pi k_b$, $\hat{\beta}_j = 0^\circ$

Nodal diameter (m,n)	One radial rotating spring	Two symmetric fixed radial springs p_m	Predicted instabilities $\left(\frac{p_m + p_n}{m+n}\right), \left(\frac{p_m + p_n}{\lvert m-n\rvert}\right)$
2	Principal: Yes	Splits: 2.68, 3.21	$(2.68+2.68)/4 = 1.34$ $(2.68+3.21)/4 = 1.47$ $(3.21+3.21)/4 = 1.61$
3	Principal: Yes	Splits: 7.58, 7.82	$(7.58+7.58)/6 = 2.53$ $(7.58+7.82)/6 = 2.57$ $(7.82+7.82)/6 = 2.61$
2,3	Combination: Yes		$(2.68+7.58)/5 = 2.05$ $(2.68+7.58)/1 = 10.26$ $(2.68+7.82)/5 = 2.10$ $(2.68+7.82)/1 = 10.50$ $(3.21+7.58)/5 = 2.16$ $(3.21+7.58)/1 = 10.79$ $(3.21+7.82)/5 = 2.21$ $(3.21+7.82)/1 = 11.03$

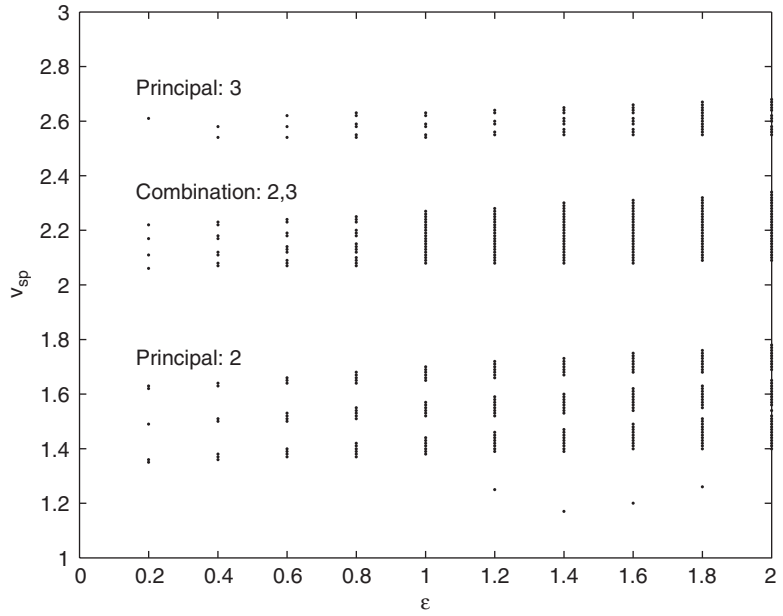

Fig. 9. Parametric instability regions for one radial rotating spring with $k_{11}=0$, $k_{21}=k, \beta_1=0^\circ$ and two radial symmetric fixed springs with $\hat{k}_{1j}=0$, $\hat{k}_{2j}=2\pi k_b, \hat{\beta}_j=0^\circ$.

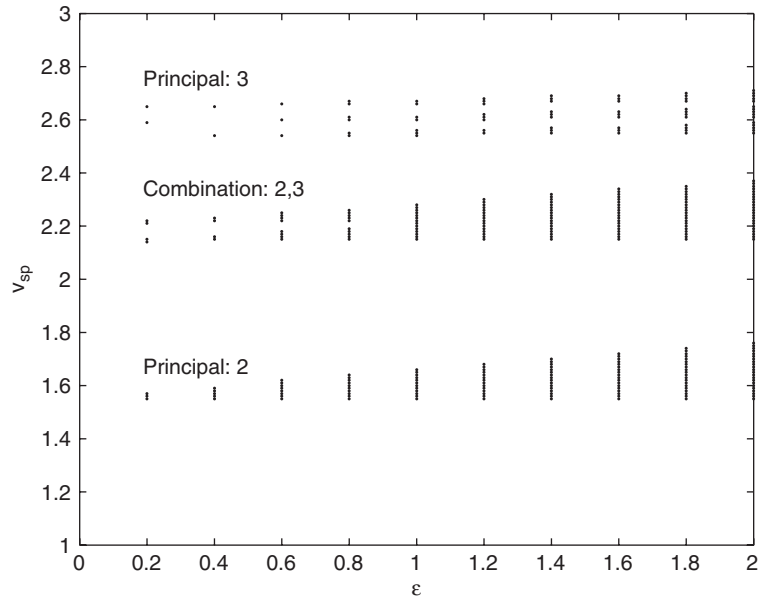

Fig. 10. Parametric instability regions for one radial rotating spring with $k_{11}=0, k_{21}=k, \beta_1=0^\circ$ and three radial symmetric fixed springs with $\hat{k}_{1j}=0$, $\hat{k}_{2j}=2\pi k_b, \hat{\beta}_j=0^\circ$.

v_{sp} combination instabilities of the second kind are not shown). Similar results are presented for the case of one rotating radial spring with three symmetric fixed radial springs (Fig. 10, Table 2) and for the case of two symmetric rotating radial springs with two symmetric fixed radial springs (Fig. 11, Table 3).

The degenerate natural frequencies of a free ring split depending on the arrangement of the fixed spring-sets and are governed by Eq. (37). The existence of parametric instabilities (principal and combination) depend

Table 2
Spring rotation speeds where parametric instability regions occur with one radial rotating spring with $k_{11}=0, k_{21}=k, \beta_1=0$ and three radial symmetric fixed springs with $\hat{k}_{1j}=0, \hat{k}_{2j}=2\pi k_b, \hat{\beta}_j=0^\circ$

Nodal diameter (m,n)	One radial rotating spring	Three symmetric fixed radial springs p_m	Predicted instabilities $\left(\frac{p_m+p_n}{m+n}\right), \left(\frac{p_m+p_n}{\lvert m-n\rvert}\right)$
2	Principal: Yes	No split: 3.09	1.55
3	Principal: Yes	Splits: 7.58, 7.95	2.53, 2.59, 2.65
2,3	Combination: Yes		2.14, 2.21, 10.67, 11.04

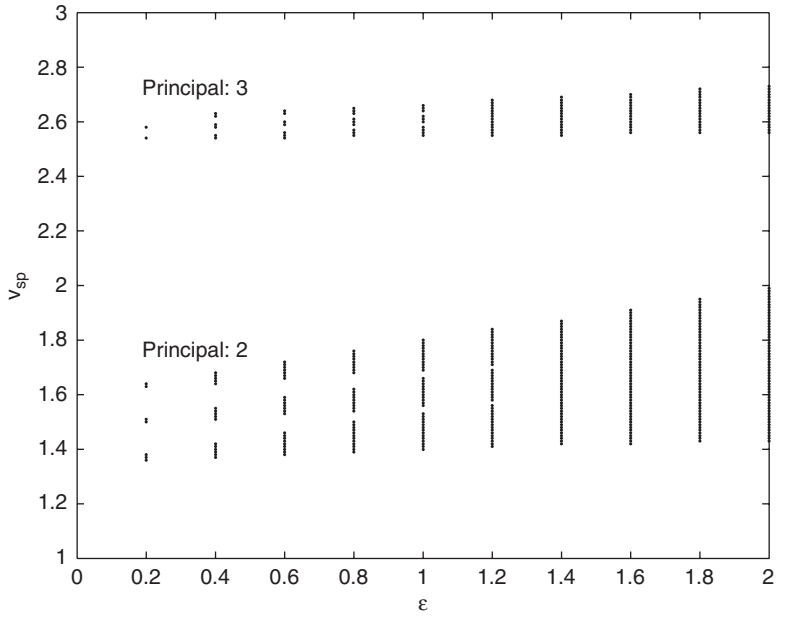

Fig. 11. Parametric instability regions for two symmetric radial rotating springs with $k_{1j}=0$, $k_{2j}=k, \beta_j=0^\circ$ and two radial symmetric fixed springs with $\hat{k}_{1j}=0$, $\hat{k}_{2j}=2\pi k_b, \hat{\beta}_j=0^\circ$.

Table 3
Spring rotation speeds where parametric instability regions occur with two symmetric radial rotating springs with $k_{1j}=0, k_{2j}=k, \beta_j=0^\circ$ and two radial symmetric fixed springs with $\hat{k}_{1j}=0, \hat{k}_{2j}=2\pi k_b, \hat{\beta}_j=0^\circ$

Nodal diameter (m,n)	One radial rotating spring	Two fixed radial springs p_m	Predicted instabilities $\left(\frac{p_m+p_n}{m+n}\right), \left(\frac{p_m+p_n}{\lvert m-n\rvert}\right)$
2	Principal: Yes	Splits: 2.68, 3.21	1.34, 1.47, 1.61
3	Principal: Yes	Splits: 7.58, 7.95	2.53, 2.57, 2.61
2,3	Combination: No		—

only on the arrangement of the rotating spring-sets, and they are governed by Eqs. (30) and (31). If the natural frequency of a particular nodal diameter mode splits because of the fixed spring-sets, then the principal as well as combination instability regions (if they exist, see the (2,3) combination instability in Table 3) associated with that nodal diameter also split.

6. Conclusions

In-plane bending vibrations of a stationary ring are parametrically excited when subject to multiple, rotating spring-sets of arbitrary stiffness and orientation. Parametric instability boundaries are obtained analytically as closed-form expressions using a first-order perturbation method. These analytical results compare well with numerical results for a practically meaningful range of the perturbation parameter. Two different methods are used for numerical verification. While both methods yield identical results, one of them is much less computationally expensive.

Although there is essentially one independent excitation frequency, namely the spring-set rotation speed v_{sp}, it is coupled to the nodal diameters m, n by projections of the spring force onto the vibration modes in Galerkin discretization. As a result, the modal coordinate equations have the parametric excitation frequencies $(m+n)v_{sp}$ and $(m-n)v_{sp}$. This generates additional instabilities. Summation combination instabilities of two kinds occur corresponding to two different values of v_{sp}: one at lower frequency $(p_m + p_n)/(m+n)$ and another at higher frequency $(p_m + p_n)/(m-n)$. Difference type instabilities do not exist for this problem.

The stiffness, orientation, and relative spacing between spring-sets govern the occurrence and width of the instability regions. Equally spaced, identical spring-sets and diametrically opposed, identical spring-sets are shown to suppress several of the instabilities. Simple rules relating the nodal diameters of the suppressed instabilities and the number of spring-sets are stated. This result has practical implications and demonstrates the advantages symmetry can play in physical systems.

Instability results for a ring with simultaneous fixed and rotating spring-sets appear like the superposition of two individual problems, one with only fixed spring-sets, and another with only rotating spring-sets. It is previously known that the degenerate natural frequencies of a ring with only fixed spring-sets split depending on the spring-set parameters (number and relative spacing). For the combined problem, parametric instability regions that occur due to rotating spring-sets in the absence of fixed supports are further split into multiple regions according to how the fixed spring-sets split the natural frequencies.

References

[1] R. Hoppe, The bending vibration of a circular ring, *Crelles Journal of Mathematics* 73 (1871) 158.
[2] A.E.H. Love, *A Treatise of the Mathematical Theory of Elasticity, 1927*, Dover, New York, NY, 1944.
[3] B.S. Seidel, E.A. Erdelyi, On the vibration of a thick ring in its own plane, *Journal of Engineering for Industry* 86 (1964) 240–244.
[4] D.A. Evensen, Nonlinear flexural vibrations of thin circular rings, *Journal of Applied Mechanics* 33 (1966) 553–560.
[5] S.S. Rao, V. Sundararajan, In-plane flexural vibrations of circular rings, *Journal of Applied Mechanics* 91 (3) (1969) 620–625.
[6] D.L. Hawkings, A generalized analysis of the vibration of circular rings, *Journal of Sound and Vibration* 54 (1) (1977) 67–74.
[7] J. Kirkhope, Simple frequency expression for the in-plane vibration of thick circular rings, *Journal of the Acoustical Society of America* 59 (1) (1976) 86–89.
[8] J. Kirkhope, In-plane vibration of a thick circular ring, *Journal of Sound and Vibration* 50 (2) (1977) 219–227.
[9] W. Kuhl, Measurements to the theories of resonant vibrations of circular rings of arbitrary wall thickness, *Akustiche Zeitschrift* 7 (1942) 10.
[10] J.W. Lincoln, E. Volterra, Experimental and theoretical determination of frequencies of elastic toroids, *Engineering Mechanics* 24 (1967) 211–217.
[11] S.S. Rao, Three-dimensional vibrations of a ring on an elastic foundation, *The Aeronautucal Journal of the Royal Aeronautical Society* 75 (1971) 417–419.
[12] X. Wu, R. G. Parker, Vibration of rings on a general elastic foundation, *Journal of Sound and Vibration* (submitted).
[13] S.C. Huang, W. Soedel, Effect of coriolis acceleration on the free and forced in-plane vibrations of rotating rings on elastic foundation, *Journal of Sound and Vibration* 115 (2) (1987) 253–274.
[14] S.C. Huang, W. Soedel, Response of rotating rings to harmonic and periodic loading and comparison with the inverted problem, *Journal of Sound and Vibration* 118 (2) (1987) 253–270.
[15] A.V. Metrikin, M.V. Tochilin, Steady-state vibrations of an elastic ring under moving load, *Journal of Sound and Vibration* 232 (3) (2000) 511–524.
[16] C.D. Mote Jr., Stability of circular plates subjected to moving loads, *Journal of the Franklin Institute* 290 (4) (1970) 329–344.
[17] W.D. Iwan, K.J. Stahl, The response of an elastic disk with a moving mass system, *Journal of Applied Mechanics* 40 (2) (1973) 445–451.
[18] W.D. Iwan, T.L. Moeller, The stability of a spinning elastic disk with a transverse load system, *Journal of Applied Mechanics* 43 (3) (1976) 485–490.

[19] I.Y. Shen, C.D. Mote Jr., On the mechanisms of instability of a circular plate under a rotating spring-mass-dashpot system, *Journal of Sound and Vibration* 148 (2) (1991) 307–318.
[20] I.Y. Shen, C.D. Mote Jr., Parametric resonances of a circular plate with inclusion subjected to a rotating spring, *Journal of Sound and Vibration* 149 (1) (1991) 164–169.
[21] I.Y. Shen, C.D. Mote Jr., Parametric excitation under multiple excitation parameters: Asymmetric plates under a rotating spring, *International Journal of Solids and Structures* 29 (8) (1992) 1019–1032.
[22] W. Soedel, *Vibrations of Shells and Plates*, Marcel Dekker, Inc, New York, NY, 1981.
[23] D.O. Brush, B.O. Almroth, *Buckling of Bars, Plates and Shells*, McGraw-Hill, New York, 1975.
[24] G.J. Simitses, *Introduction to the Elastic Stability of Structures*, Prentice-Hall, Inc, New Jersey, 1976.
[25] W. Kim, J. Chung, Free non-linear vibration of a rotating thin ring with the in-plane and out-of-plane motions, *Journal of Sound and Vibration* 258 (1) (2002) 167–178.